The Astrophysical Journal, 697:L38–L43, 2009 May 20 doi:10.1088/0004-637X/697/1/L38

GRAVITATIONAL HEATING HELPS MAKE MASSIVE GALAXIES RED AND DEAD

Peter H. Johansson[1], Thorsten Naab[1], and Jeremiah P. Ostriker[2]
[1] Universitäts-Sternwarte München, Scheinerstr. 1, D-81679 München, Germany; pjohan@usm.lmu.de
[2] Department of Astrophysics, Peyton Hall, Princeton, NJ, USA
Received 2009 March 16; accepted 2009 April 14; published 2009 April 29

ABSTRACT

We study the thermal formation history of four simulated galaxies that were shown by Naab et al. to reproduce a number of observed properties of elliptical galaxies. The temperature of the gas in the galaxies is steadily increasing with decreasing redshift, although much of the gas has a cooling time shorter than the Hubble time. The gas is being heated and kept hot by gravitational heating processes through the release of potential energy from infalling stellar clumps. The energy is dissipated in supersonic collisions of infalling gas lumps with the ambient gas and through the dynamical capturing of satellite systems causing gravitational wakes that transfer energy to the surrounding gas. Furthermore, dynamical friction from the infalling clumps pushes out dark matter (DM), lowering the central DM density by up to a factor of 2 from $z = 3$ to $z = 0$. In galaxies in which the late formation history ($z \lesssim 2$) is dominated by minor merging and accretion, the energy released ($E \sim 5 \times 10^{59}$ erg) from gravitational feedback is sufficient to form red and dead elliptical galaxies by $z \sim 1$ even in the absence of supernova and AGN feedback.

Key words: galaxies: elliptical and lenticular, cD – galaxies: evolution – galaxies: formation – methods: numerical

1. INTRODUCTION

In the standard cold dark matter (CDM) picture of galaxy formation, gas falling into dark matter (DM) halos is shock-heated approximately to the halo virial temperature, $T_{\rm vir} = 10^6\ (v_{\rm circ}/167\ {\rm km\ s^{-1}})$ K maintaining quasi-hydrostatic equilibrium with the DM component (Rees & Ostriker 1977; Binney 1977; Silk 1977; White & Rees 1978). The gas will cool, losing its pressure support, and settling into a centrifugally supported disk while conserving its specific angular momentum (Fall & Efstathiou 1980). However, recently, Birnboim & Dekel (2003) and Dekel & Birnboim (2006) showed using one-dimensional models that galaxy halos can only shock-heat infalling gas if the cooling rate for gas behind the shock is lower than the compression rate of the infalling gas. This criterion translates to a roughly redshift-independent critical minimum mass for halos that are able to shock-heat the infalling gas of $M_{\rm shock} \approx 10^{11.6} M_\odot$. Less massive halos are not able to support stable shocks and the majority of their gas is accreted cold. However, in the general three-dimensional case, galaxies above the critical shock mass can also be fed with cold gas along filaments penetrating deep inside the hot halo (Ocvirk et al. 2008).

Recent simulations also predict that the baryonic growth of most galaxies is dominated by smooth accretion events of either hot or cold gas, as opposed to individual merger events (Genel et al 2008; Brooks et al. 2009). Observations of massive star-forming galaxies at $z \sim 2$ have found a preponderance for thick gas-rich rotating disks with large turbulent motions and only a minority of major mergers (Förster Schreiber et al. 2006; Shapiro et al. 2008). The observed high-redshift disks exhibit large turbulent motions that could potentially be the result of gravitational energy release from cold accretion flows feeding the galaxy (Genzel et al. 2008). Given the bimodal temperature distribution of the accreted gas and the characteristic mass scale of $M_{\rm shock}$, it is tempting to link this to the observed bimodality in the galaxy population dividing them into a red and blue sequence with a critical stellar mass of $M_{\rm crit} \simeq 3 \times 10^{10}\ M_\odot$, which was revealed in recent large galaxy surveys (e.g., Bell et al. 2003; Kauffmann et al. 2003). Galaxies below this critical mass are typically blue, star-forming disk galaxies, whereas galaxies above $M_{\rm crit}$ are dominated by red spheroidal systems with old stellar populations.

The observed bimodality can be explained if star formation in halos above a critical threshold mass of $M \sim 10^{12}\ M_\odot$ is suppressed (e.g., Bower et al. 2006; Cattaneo et al. 2006). The quenching mechanism needs to be both energetic enough to trigger the quenching and long-lasting enough to maintain the quenching over a Hubble time. In addition to the quenching by shock-heated gas above a critical halo mass (Dekel & Birnboim 2006; Birnboim et al. 2007), potential quenching mechanisms include the feedback from active galactic nuclei (AGNs; Ciotti & Ostriker 2007), gaseous major mergers triggering starburst and/or quasar activity (e.g., Naab et al. 2006; Hopkins et al. 2007; Johansson et al. 2009) and gravitational quenching by clumpy accretion (Dekel & Birnboim 2008). Environmental effects and the input of gravitational energy from infalling clumps are real and automatically included in high-resolution numerical simulations. In semi-analytic models these environmental effects are not usually included (see, however, Khochfar & Ostriker 2008 for an exception).

In this Letter, we study in detail the thermal formation history of a set of very high resolution cosmological re-simulations of individual galaxies. In an earlier paper (Naab et al. 2007, hereafter N07), we showed that the simulated galaxies reproduce a number of observed properties of elliptical galaxies, although the simulations include neither stellar nor AGN feedback. We show that the gas is heated and kept hot by gravitational feedback, efficiently terminating star formation and leading to the formation of systems with evolved stellar populations and low star formation rates by $z \sim 1$. Gravitational feedback comes in many forms. Incoming lumps or streams of cold gas ultimately come to rest depositing their potential energy frictionally (i.e., through decaying turbulence). Supersonic collisions of infalling gas with the ambient gas lead to propagating shock waves (Ryu et al. 2003) which also deposit entropy throughout the system. Gradual accretion to the gaseous envelope of the galaxy adds weight, causing contraction and PdV work on the ambient gas. And finally infalling satellite systems captured through dynamical friction cause gaseous wakes from which energy is transferred to the surrounding gas (Ostriker 1999). These are all

Table 1
Galaxy Properties Within $r_{\rm vir}$ at $z = 0$

Galaxy	$M_{\rm vir}$[a]	$M_{\rm stars}$	$M_{\rm gas}$	$M_{\rm DM}$	$r_{\rm vir}$[b]	$v_{\rm max}$[c]
A1	169	21.7	13.3	134	258	270
C1	125	17.2	9.3	98.5	233	258
E1	134	19.0	9.3	106	239	307
A2	179	22.8	11.6	145	263	232

Notes.
[a] Total masses M in $10^{10}\,M_\odot$.
[b] Virial radius in kpc, defined as the radius enclosing an overdensity of 200 times the critical density $\rho_{\rm crit}$.
[c] Maximum circular velocity in km s^{-1}.

variants of the processes by which gravitational energy released by infalling matter can be transferred to the gas maintained in quasi-hydrostatic equilibrium within galaxies, heating it and tending to counteract radiative losses.

2. SIMULATIONS

The ΛCDM initial conditions assume scale-invariant adiabatic fluctuations with $\Gamma = 0.2$ (Efstathiou et al. 1992). Throughout this Letter, we use a *WMAP-1* (Spergel et al. 2003) cosmology with a slightly lower Hubble parameter of $h = 0.65$[3] with $\sigma_8 = 0.86$, $f_b = \Omega_b/\Omega_m = 0.2$, $\Omega_0 = 0.3$, and $\Lambda_0 = 0.7$. The galaxies were simulated at high resolution using the volume renormalization technique (Katz & White 1993) by selecting target halos at $z = 0$ in low-density environments from a low-resolution DM simulation. In the re-simulations, the particle number of the gas and DM particles was increased to 100^3 (Halos A1, C, and E) and 200^3 (Halo A2) within a cubic volume at redshift $z = 24$ containing all the particles that ended up within the virialized region of the halos at $z = 0$. The virial properties of the galaxies at $z = 0$ are summarized in Table 1.

The simulations were performed using the TreeSPH-code GADGET-2 (Springel 2005) on shared-memory machines hosted in Cambridge, Munich, and Princeton. The code includes star formation and optically thin radiative cooling for a primordial composition of hydrogen and helium (Katz et al. 1996). We included a spatially uniform redshift-dependent UV background radiation field with a modified (Haardt & Madau 1996) spectrum. We modify the self-regulated feedback model of Springel & Hernquist (2003) by turning off the feedback from supernovae, eliminating the two-phase description of the interstellar medium (ISM) of star-forming particles with $\rho > \rho_{\rm thresh}$ (McKee & Ostriker 1977; Johansson & Efstathiou 2006), and thus transforming their entire gas component into the cold phase with a pre-set temperature of $T_{\rm cold} = 1000$ K. The star formation timescale is set by $t_\star = t_0^\star(\rho_{\rm thresh}/\rho)^{1/2}$, where we set the free parameters to $t_0^\star = 1.5h^{-1}$ Gyr and $\rho_{\rm thresh} = 7 \times 10^{-26} h^2$ g cm^{-3}.

The gravitational softening length for the 100^3 (200^3) runs was fixed in comoving units of $\epsilon_{\rm gas} = \epsilon_\star = 0.25$ (0.125) kpc and $\epsilon_{\rm DM} = 0.5$ (0.25) kpc until $z = 9$, after which the softening remained fixed in physical coordinates at the same values. Our lowest (highest) resolution runs have particle masses of $m_{\rm stars} = 1.05 \times 10^6\ M_\odot$ ($m_{\rm stars} = 1.3 \times 10^5\ M_\odot$), $m_{\rm gas} = 2.1 \times 10^6\ M_\odot$ ($m_{\rm gas} = 2.6 \times 10^5\ M_\odot$), and $m_{\rm dm} = 8.2 \times 10^6\ M_\odot$ ($m_{\rm dm} = 1.03 \times 10^6\ M_\odot$) for the stars, gas, and DM, respectively.

[3] h is defined such that $H_0 = 100h$ km s^{-1} Mpc^{-1}.

3. GRAVITATIONAL HEATING

3.1. Temperature Structure of the Gas

We summarize the evolution of the gas temperature at redshifts $z = 0, 1, 4$ for our model galaxies in Figure 1 by showing the temperature profiles (left panel), the entropy distributions (middle panel), and the phase-space diagrams (right panel) of all gas within the virial radius. The temperature of the gas is increasing in all galaxies with decreasing redshift reaching $T \sim 10^6$ K at $z = 0$, with cool, star-forming gas only found at the very centers of the galaxies. In the middle panel, we plot the distribution of the gas entropy, defined as $S = kTn^{-2/3}$ and define the cooling time of the gas as

$$t_{\rm cool} = \left(\frac{S}{10\ {\rm keV\ cm^2}}\right)^{3/2} \frac{1.5(\mu_e/\mu)^2 \cdot (10\ {\rm keV\ cm^2})^{3/2}}{(kT)^{1/2}\Lambda(T, Z)}, \quad (1)$$

where k is the Boltzmann constant, $\Lambda(T, Z)$ is the cooling function, and $\mu \simeq 0.59$, $\mu_e \simeq 1.1$ for a fully ionized gas. The first term is a measure of the entropy and therefore an adiabatic invariant, whereas the second term only depends on the temperature (T) and metallicity (Z) of the gas (Scannapieco & Oh 2004; Khalatyan et al. 2008). The second factor in Equation (1) has an absolute minimum, corresponding to $t_{\rm cool} \sim 2$ Gyr for our primordial cooling function (and $S = 10$ keV cm^2, with different S corresponding to different $t_{\rm cool}$). We plot in Figure 1 the entropy values corresponding to minimum cooling times of 0.1, 1, and 10 Gyr as dashed lines. At high redshifts the entropy distribution of the gas is bimodal with cold, high-density, star-forming gas forming a low entropy peak and lower density, hot shock-heated gas forming a high entropy peak. At lower redshifts, the available low entropy gas has been consumed by star formation and we are primarily left with dilute shock-heated gas with cooling times of the order of $t_{\rm cool} \sim$ 5–10 Gyr.

At high redshifts ($z \gtrsim 4$), the gas flows into the galaxies predominantly in the cold phase with the hot gas (defined as $T > 2.5 \times 10^5$ K) fraction being low at $f_{\rm hot} \lesssim 30\%$. A large fraction of the gas can also be found in the cold star-forming phase. With decreasing redshift, the fraction of hot gas steadily increases; by $z \sim 3$ the hot gas fraction is around $f_{\rm hot} \sim 50\%$. The transition from a cold gas accretion mode to a hot-gas-dominated accretion mode occurs at $z \sim$ 2–3, corresponding to halo masses of $M_{\rm halo} = 3$–$5 \times 10^{11}\ M_\odot$ in good agreement with the predictions of Dekel & Birnboim (2006), see also Kereš et al. (2005). Below these redshifts, the galaxy halos are massive enough to support stable shocks and most of the accreted gas is shock-heated close to the virial temperature of the halos. As this transition is mass dependent, it occurs somewhat earlier in the more massive halo A1, compared to the slightly lower mass halos C and E. At $z = 0$ the hot gas fraction is $f_{\rm hot} \gtrsim 97\%$, with only some residual cold star-forming gas remaining, as most of the original gas has either formed stars or been shock-heated to high temperatures.

3.2. Gravitational Energy Input

The diffuse gas is heated by gravitational feedback in the form of gravitational energy release from infalling stellar and gaseous clumps. We quantify this effect in Figure 2 which shows the cumulative change of the binding energies ($\Sigma(\Delta E_{\rm bind})$) of in situ (circles) and accreted (squares) stars within a fixed radius of $r < 30$ kpc. In situ stars are defined as stars that were born from gas in the galaxy ($r < 30$ kpc), whereas accreted

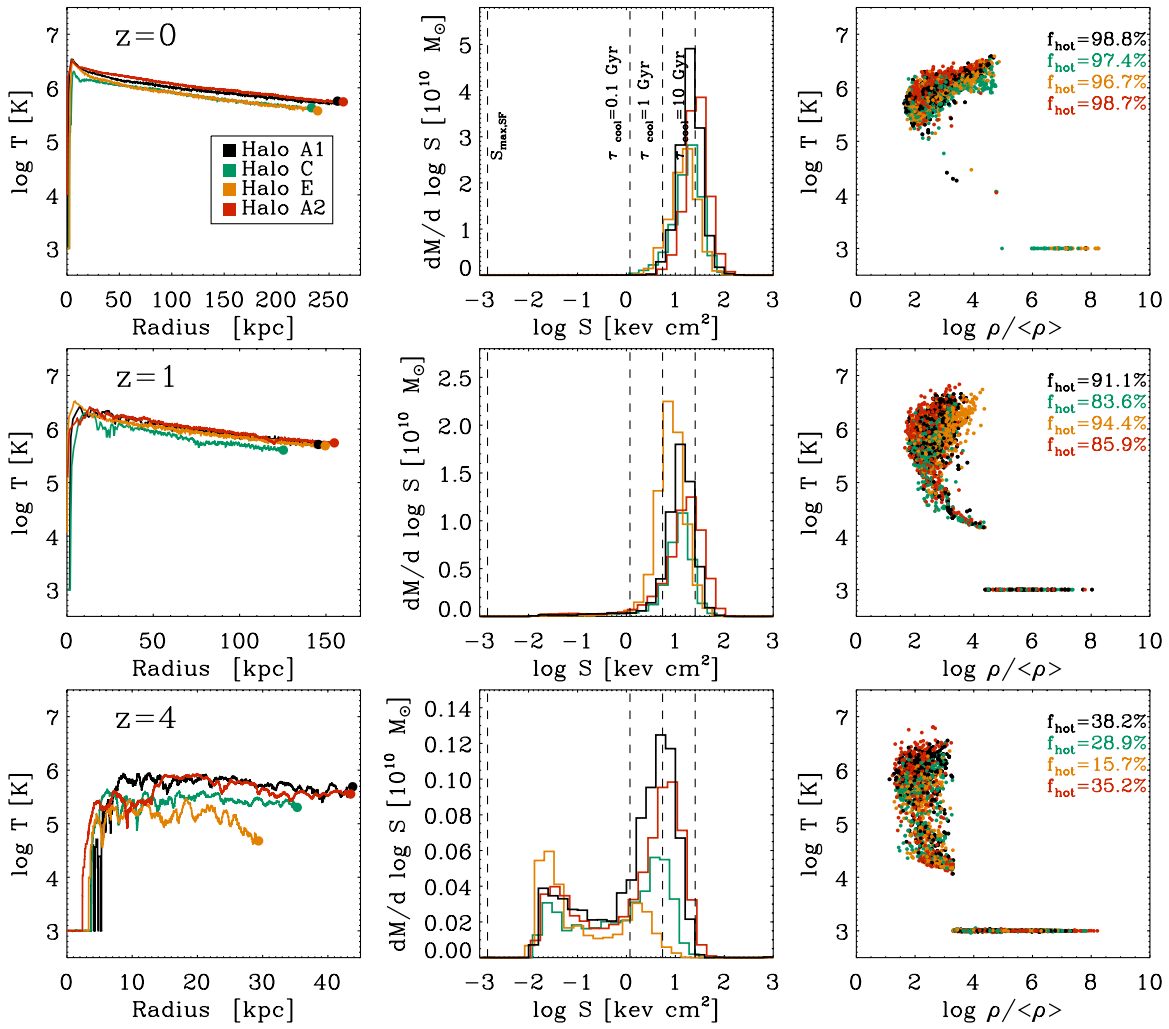

Figure 1. Evolution of the temperature profile (left panel), the entropy distribution (middle panel), and the phase-space diagram (right panel) of all gas within $r_{\rm vir}$ as a function of redshift (top to bottom) for halos A1 (black), C (green), E (orange), and halo A2 (red), where $f_{\rm hot}$ is the fraction of gas with $T > 2.5 \times 10^5$ K. Even though much of the gas has a cooling time shorter than the Hubble time its temperature steadily increases due to the enumerated gravitational heating processes.

stars have formed outside the galaxy and have been accreted later on. The $\Sigma_{\rm ins}(\Delta E_{\rm bind})$ reflects the overall mass growth and deepening of the potential well, whereas $\Sigma_{\rm acc}(\Delta E_{\rm bind})$ describes the release of gravitational energy from accreted structures. All of the energy released by the growth of the potential energy of the accreted stars ($E_{\rm bind} \sim 5 \times 10^{59}$ erg) goes into heating the gas and moving outwards DM and previous generations of stars (on average ~5%–10% of the released energy ends up as kinetic energy of the stars), whereas much of the energy release associated with the potential energy growth of the in situ stars is radiated away.

All galaxies assemble rapidly at high redshifts ($z = 5$–3) with $\Sigma\Delta(E_{\rm bind})$ of both the in situ and accreted stars increasing by an order of magnitude. The change in the accreted $\Sigma_{\rm acc}(\Delta E_{\rm bind})$ mirrors the mass accretion history of the galaxies with the 3:1 merger for Galaxy C at $z = 0.6$ and the nearly 1:1 merger for Galaxy E at $z = 1.5$ clearly visible (see Figure 7 in N07 for details). At $z < 1$ the integrated change in the potential energy is dominated by accreted stars for halos A1, C, A2 (dissipationless formation), and in situ stars for halo E (dissipational formation), with the binding energy/atom increasing by ~20% from $z = 1$ to $z = 0$. The $\Sigma_{\rm acc}(\Delta E_{\rm bind})$ is 2–3 times larger compared to $\Sigma_{\rm ins}(\Delta E_{\rm bind})$ for halos A1, C, and A2 at $z < 1$, whereas halo E is dominated by in situ star formation and $\Sigma_{\rm ins}(\Delta E_{\rm bind})$ is a factor

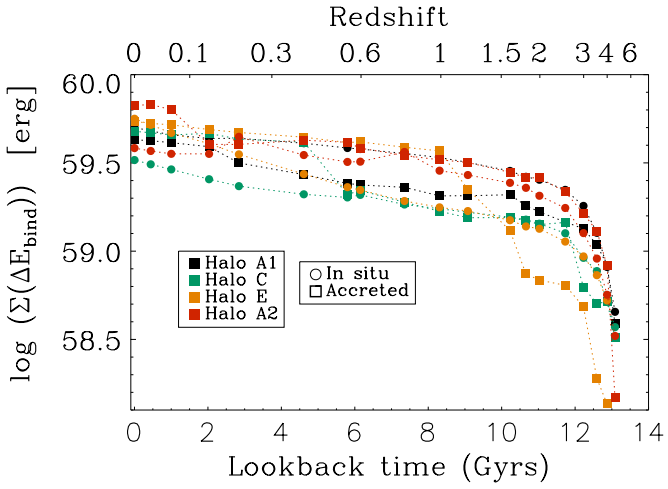

Figure 2. Cumulative change in binding energy $\Delta E_{\rm bind}$ summed from $z = 5$ to $z = 0$ separately for in situ (circles) and accreted stars (squares) as a function of lookback time (redshift).

of 4 larger than $\Sigma_{\rm acc}(\Delta E_{\rm bind})$. We expect gravitational feedback effects to be important in the galaxies assembled through dissipationless processes (A1, C, A2), whereas gravitational

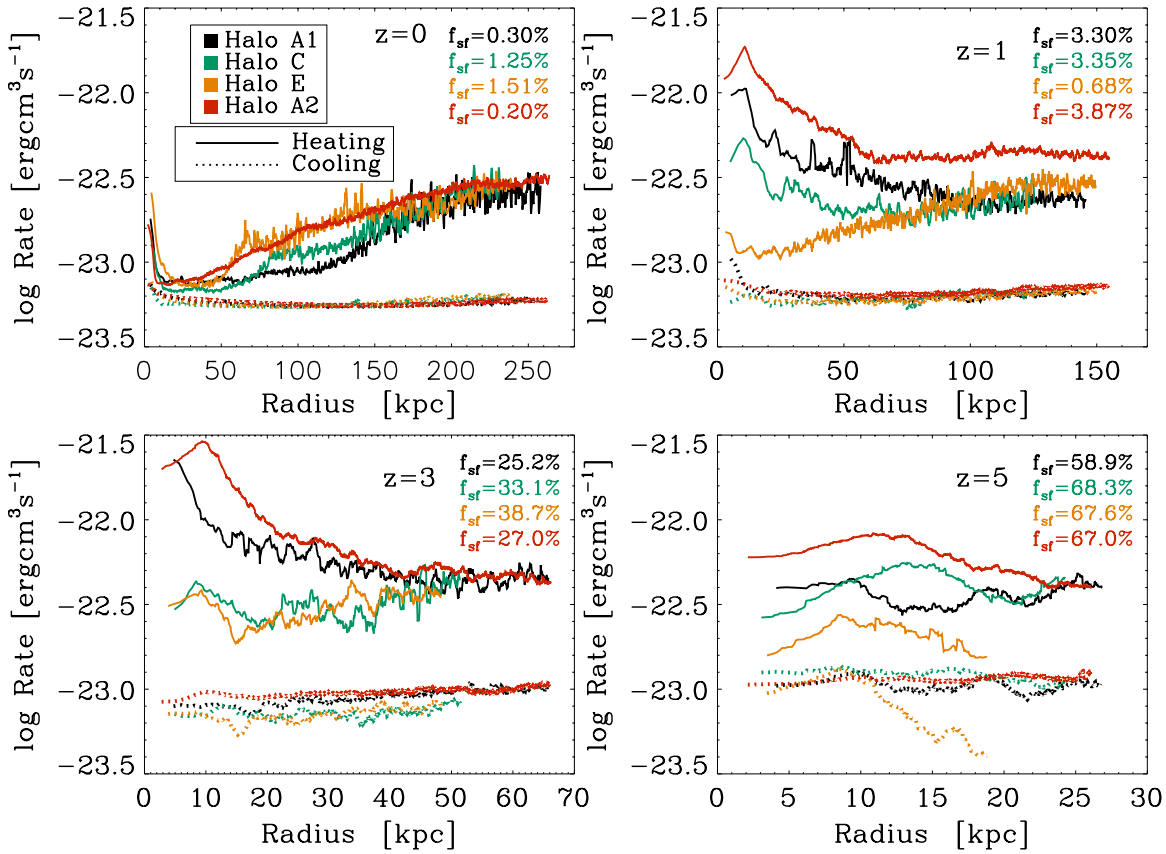

Figure 3. Net heating (solid line) and net cooling rates (dashed lines) for non-star-forming ($\rho < \rho_{\rm thresh}$) gas within $r_{\rm vir}$ at redshifts 0, 1, 3, and 5 for the four halos. The fraction $f_{\rm sf}$ of dense star-forming gas ($\rho > \rho_{\rm thresh}$) is also given. The heating rate dominates over the cooling rate at all redshifts for the low-density non-star-forming gas.

feedback plays a minor role in the dissipational formation of galaxy E. We also see a trend with increasing resolution, the final $\Sigma_{\rm acc}(\Delta E_{\rm bind})$ of halo A2 is higher by 50%, whereas the $\Sigma_{\rm ins}(\Delta E_{\rm bind})$ is lower by 30% compared to halo A1. Thus, we expect stronger gravitational feedback effects with increasing resolution as we are able to resolve smaller structures.

3.3. Heating of the Gas Component

The energy input from gravitational feedback scales with the mass fraction of each component, with roughly $\Omega_b/(\Omega_m + \Omega_b) = 1/6$ and $\Omega_m/(\Omega_m + \Omega_b) = 5/6$ going into the baryonic and DM components, respectively. Accreted lumps and cold streams of gas deposit energy into the gas through dissipation of turbulence. The infalling clumps have typical velocities of $v_{z=0} \sim 400$ km s^{-1}, $v_{z=3} \sim 200$ km s^{-1}, $v_{z=5} \sim 100$ km s^{-1} as estimated from the difference of the escape velocity at $r_{\rm vir}$ and $0.1r_{\rm vir}$. The corresponding sound speeds of the ambient gas are $c_{z=0} \sim 150$ km s^{-1}, $c_{z=3} \sim 100$ km s^{-1}, $c_{z=5} \sim 20$ km s^{-1} resulting typically in weak shocks with Mach numbers of 2–5.

We quantify this effect by studying the terms of the entropy equation of GADGET-2 for a given particle i (Springel & Hernquist 2002):

$$\frac{dA_i}{dt} = -\frac{\gamma - 1}{\rho_i^{\gamma}}\Lambda(\rho_i, u_i) + \frac{1}{2}\frac{\gamma - 1}{\rho_i^{\gamma}}\sum_{j=1}^{N} m_j \Pi_{ij} \mathbf{v_{ij}} \cdot \nabla_i \bar{W}_{\rm ij}. \quad (2)$$

Here the first term depicts the external radiative cooling (or heating) of the gas and the second term gives the generation of entropy by artificial viscosity in shocks and where the internal energy is defined as $u = A/(\gamma - 1)\rho^{\gamma - 1}$. In Figure 3, we plot the cooling and heating rates derived from Equation (2) for all non-star-forming gas ($\rho < \rho_{\rm thresh}$) for our four galaxies at redshifts $z = 0, 1, 3, 5$. The fraction of dense star-forming gas ($\rho > \rho_{\rm thresh}$) at $T = 1000$ K that is not participating in the cooling/heating process is also given in the figure. The shock-induced heating rate of the diffuse gas is larger at all redshifts compared to the cooling rate. At large redshifts, a substantial fraction of the gas ($\sim$2/3 at $z = 5$) and ($\sim$1/3 at $z = 3$) is star forming, whereas at $z \lesssim 1$ this fraction is below a few percent. At $z \lesssim 1$ the energy input from gravitational feedback is able to keep the gas hot in the galaxies forming dissipationlessly (A1, C, A2), whereas the dissipationally forming galaxy E exhibits much lower heating rates at $z = 1$.

3.4. Heating of the Dark Matter Component

In addition to heating the gas the gravitational feedback heats the DM of the galaxies causing it to expand outwards. We quantify this effect in Figure 4, where we plot the central DM mass within $r < 2$ kpc in our four galaxies (circles) as a function of lookback time. The employed gravitational softening ($\epsilon = 0.25$–0.5 kpc) is a Plummer equivalent Spline softening length, for which the force is exactly Newtonian beyond $h = 2.8\epsilon$. Thus, $r < 2$ kpc is resolved by 4–8 $\times\ \epsilon$, which should be sufficient to follow the DM mass evolution reliably.

In the galaxies that form dissipationlessly we see an initial increase in the central DM due to adiabatic contraction. After a peak DM mass at $z = 3$, the central DM mass steadily declines

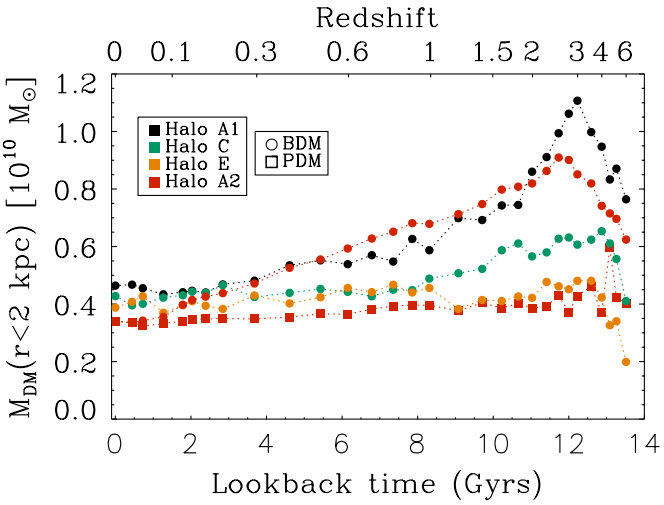

Figure 4. Cumulative DM mass distribution within $r < 2$ kpc as a function of lookback time (redshift). The circles give the DM mass in our full baryons + DM (BDM) runs and the squares the DM mass in a pure DM (PDM) simulation of halo A2.

due to heating from infalling clumps, with the final central DM mass being a factor of 2 lower for galaxies A1, A2 and 50% lower for galaxy C. In contrast, galaxy E shows a constant evolution of the central DM mass, with the $z = 0$ and $z = 3$ central DM masses being roughly the same. We also plot for comparison the central DM of a pure DM (PDM) simulation of halo A2 at 200^3 resolution (red squares). For the PDM simulation, we see neither the adiabatic contraction phase nor the pushing out of DM, thus resulting in a constant central DM mass throughout the simulation.

This has important implications for the recent estimates of central DM content of elliptical galaxies (e.g., Thomas et al. 2009). The gravitational energy release from infalling clumps might help in transforming an initially cuspy DM profile to a cored profile as seen in our simulations (see also El-Zant et al. 2001; Romano-Díaz et al. 2008, 2009). Furthermore, once a cored DM profile with a hot low-density gas halo is in place, it can be maintained through the infall of cold gas clouds even without the inclusion of additional feedback sources (Kaufmann et al. 2008). Finally, the accretion of minor mergers can potentially explain the strong size evolution observed in elliptical galaxies between $z = 2$–0 (van Dokkum et al. 2008; Naab et al. 2009).

4. DISCUSSION

In this Letter, we have studied the formation history of four galaxies that reproduce a number of observed properties for elliptical galaxies. We have shown that for three galaxies (A1, C, A2) for which the late formation ($z \lesssim 2$) is dominated by dissipationless minor merging that the energy release from gravitational feedback alone is sufficient to make these galaxies red and dead by $z = 1$, the fourth galaxy (E) has a dissipational formation history with significant ongoing star formation at low redshifts. Stellar and AGN feedback are both real and important, especially in driving winds and outflows that enrich the intergalactic medium with metals (e.g., Oppenheimer & Davé 2006) and potentially in determining the lower and upper cutoffs in the observed galaxy luminosity function (Benson et al. 2003). Furthermore, the baryon/DM fraction in our simulated galaxies is a factor of 2 too high for their mass compared to predictions from recent lensing data (Mandelbaum et al. 2006). However, in order to isolate the effects of gravitational heating from infalling clumps, which would occur even if there were neither stellar nor AGN feedback, we chose to run our simulations without any additional energy feedback.

The efficiency of gravitational feedback can be estimated using the following simple argument,

$$\frac{d\phi}{dr} = -\frac{Gm_0}{r_0}\frac{1}{r} = -\frac{v_c^2}{r} \Rightarrow \Delta\phi(r) = -v_c^2 \log(\frac{r_{\rm vir}}{r}), \quad (3)$$

where the final change in potential energy results from integrating from $r_{\rm vir}$ to a fiducial infall radius r. Gravitational feedback energy $(\Delta E)_{\rm grav} = \Delta m_\star \Delta\phi(r)$ resulting in

$$(\Delta E)_{\rm grav} = \Delta m_\star v_c^2 \log(100) \sim 4.5 \times 10^{-6} v_{300}^2 m_\star c^2, \quad (4)$$

where $r_{\rm vir}/r = 100$ and v_{300} is the circular velocity in units of 300 km s^{-1}. Inserting the values for galaxy A1 at $z = 0$ ($v = 271$ km s^{-1} and $m_\star = 1.23 \times 10^{11}\ M_\odot$) into Equation (4) results in $(\Delta E)_{\rm grav} \sim 8 \times 10^{59}$ erg which is remarkably similar to the values that can be read off Figure 2. More importantly, this energy is of the same order as the feedback energy from supernova II $(\Delta E)_{\rm SNII} \sim 2.8 \times 10^{-6} m_\star c^2$ (for a Salpeter IMF and 10^{51} erg per supernova) and AGN feedback energy $(\Delta E)_{\rm AGN} \sim 5 \times 10^{-6} m_\star c^2$ (for $m_{\rm BH}/m_\star = 10^{-3}$ and a total AGN feedback efficiency of 0.5%). However, unlike SNII and AGN feedback energy, gravitational feedback energy scales with $(\Delta E)_{\rm grav} \propto v_c^2$, making it proportionally more important in massive systems with large circular velocities. Furthermore, the energy released from gravitational feedback is distributed throughout the galaxy halo, whereas the feedback energy from SNII and AGN feedback is confined to the central region of the halo in regions with high-density cold gas that can efficiently radiate away the energy.

The process presented here is general, but in detail might depend on the implementation of additional feedback. The inclusion of supernova feedback might be important in lowering the number of stellar clumps thus decreasing the amount of gravitational feedback in the system. Another important factor not included in our simulations is metal cooling that is expected to increase the cooling rates by a factor of 10 or more. However, the increased cooling rates might to some extent be counteracted by efficient stellar and AGN feedback, especially in the central regions of the galaxies. Finally, the derived heating rates at the peak of the gravitational feedback phase ($z = 1$ in Figure 3) are typically 15–20 times higher than the cooling rate of gas with primordial composition and thus gravitational feedback energy is expected to be an important energy source in the dissipationless formation process of all massive galaxies.

We thank G. Efstathiou for stimulating discussions. This research was funded by the DFG cluster of excellence "Origin and Structure of the Universe."

REFERENCES

Bell, E. F., McIntosh, D. H., Katz, N., & Weinberg, M. D. 2003, ApJS, 149, 289
Benson, A. J., et al. 2003, ApJ, 599, 38
Binney, J. 1977, ApJ, 215, 483
Birnboim, Y., & Dekel, A. 2003, MNRAS, 345, 349
Birnboim, Y., Dekel, A., & Neistein, E. 2007, MNRAS, 380, 339
Bower, R. G., et al. 2006, MNRAS, 370, 645
Brooks, A. M., Governato, F., Quinn, T., Brook, C. B., & Wadsley, J. 2009, ApJ, 694, 396

Cattaneo, A., Dekel, A., Devriendt, J., Guiderdoni, B., & Blaizot, J. 2006, MNRAS, 370, 1651
Ciotti, L., & Ostriker, J. P. 2007, ApJ, 665, 1038
Dekel, A., & Birnboim, Y. 2006, MNRAS, 368, 2
Dekel, A., & Birnboim, Y. 2008, MNRAS, 383, 119
Efstathiou, G., Bond, J. R., & White, S. D. M. 1992, MNRAS, 258, 1P
El-Zant, A., Shlosman, I., & Hoffman, Y. 2001, ApJ, 560, 636
Fall, S. M., & Efstathiou, G. 1980, MNRAS, 193, 189
Förster Schreiber, N. M., et al. 2006, ApJ, 645, 1062
Genel, S., et al. 2008, ApJ, 688, 789
Genzel, R., et al. 2008, ApJ, 687, 59
Haardt, F., & Madau, P. 1996, ApJ, 461, 20
Hopkins, P. F., Bundy, K., Hernquist, L., & Ellis, R. S. 2007, ApJ, 659, 976
Johansson, P. H., & Efstathiou, G. 2006, MNRAS, 371, 1519
Johansson, P. H., Naab, T., & Burkert, A. 2009, ApJ, 690, 802
Katz, N., Weinberg, D. H., & Hernquist, L. 1996, ApJS, 105, 19
Katz, N., & White, S. D. M. 1993, ApJ, 412, 455
Kauffmann, G., et al. 2003, MNRAS, 341, 33
Kaufmann, T., Bullock, J. S., Maller, A. H., Fang, T., & Wadsley, J. 2008, arXiv:0812.2025
Kereš, D., Katz, N., Weinberg, D. H., & Davé, R. 2005, MNRAS, 363, 2
Khalatyan, A., et al. 2008, MNRAS, 387, 13
Khochfar, S., & Ostriker, J. P. 2008, ApJ, 680, 54
Mandelbaum, R., Seljak, U., Kauffmann, G., Hirata, C. M., & Brinkmann, J. 2006, MNRAS, 368, 715
McKee, C. F., & Ostriker, J. P. 1977, ApJ, 218, 148
Naab, T., Jesseit, R., & Burkert, A. 2006, MNRAS, 372, 839
Naab, T., Johansson, P. H., & Ostriker, J. P. 2009, arXiv:0903.1636
Naab, T., Johansson, P. H., Ostriker, J. P., & Efstathiou, G. 2007, ApJ, 658, 710
Ocvirk, P., Pichon, C., & Teyssier, R. 2008, MNRAS, 390, 1326
Oppenheimer, B. D., & Davé, R. 2006, MNRAS, 373, 1265
Ostriker, E. C. 1999, ApJ, 513, 252
Rees, M. J., & Ostriker, J. P. 1977, MNRAS, 179, 541
Romano-Díaz, E., Shlosman, I., Hoffman, Y., & Heller, C. 2008, ApJ, 685, L105
Romano-Díaz, E., Shlosman, I., Hoffman, Y., & Heller, C. 2009, arXiv:0901.1317
Ryu, D., Kang, H., Hallman, E., & Jones, T. W. 2003, ApJ, 593, 599
Scannapieco, E., & Oh, S. P. 2004, ApJ, 608, 62
Shapiro, K. L., et al. 2008, ApJ, 682, 231
Silk, J. 1977, ApJ, 211, 638
Spergel, et al. 2003, ApJS, 148, 175
Springel, V. 2005, MNRAS, 364, 1105
Springel, V., & Hernquist, L. 2002, MNRAS, 333, 649
Springel, V., & Hernquist, L. 2003, MNRAS, 339, 289
Thomas, J., et al. 2009, ApJ, 691, 770
van Dokkum, P. G., et al. 2008, ApJ, 677, L5
White, S. D. M., & Rees, M. J. 1978, MNRAS, 183, 341